Operation of a 0.2-1.1 keV Ion Source within a Magnetized Laboratory Plasma

H. Boehmer, D. Edrich, W.W. Heidbrink, R. McWilliams, L. Zhao,

University of California, Irvine

D. Leneman

University of California, Los Angeles

ABSTRACT. To study the physics of energetic ions in magnetized plasma, a radio-frequency (RF) ion beam is inserted into the 1-kG, $\sim$ 3 eV, $\sim$ 10^{12} cm^{-3} plasma produced by the upgraded LArge Plasma Device (LAPD). The commercial 100-1000 eV argon source normally operates in an unmagnetized microelectronics production environment. Successful operation in the LAPD requires numerous modifications, including electrical isolation of the source housing, relocation of the matching network for the RF, reduction of the gas pressure, pulsed operation to avoid overheating, and care to preserve current neutralization in the presence of a strong magnetic field. With these modifications, a $\sim$ 500-eV, milliampere beam that propagates axially more than 6 meters is obtained.

Review of Scientific Instruments manuscript #A03708.

1. Introduction

Fast ions that have energies much larger than the thermal, bulk-ion population are pervasive in astrophysical, space, and fusion plasmas. Unfortunately, fast-ion physics studies are challenging in both space and laboratory plasmas. Detailed measurements of the plasma properties, the fast-ion velocities and spatial profile, and the spectrum of any waves or instabilities are required for a full characterization. In space, the spatial scales are daunting. In a hot fusion plasma such as a tokamak, the plasma profiles are well characterized but the high temperatures complicate measurements of the fluctuations (particularly at the most relevant, relatively long spatial scales) and fast-ion properties are inferred indirectly from external measurements. The objective of the work reported here is to develop a fast-ion source that can be inserted into a relatively cool, laboratory plasma that is accessible to probes and fast-ion diagnostics. This source is being employed in studies of wave-particle interactions and of collisional and fluctuation-induced transport of fast ions.

The upgraded LArge Plasma Device (LAPD) [1] at the University of California, Los Angeles (UCLA) is well suited for laboratory studies of fast-ion physics. The 1-m diameter, 18-m long cylindrical vacuum chamber is sufficiently large to confine fast-ion orbits. The excellent plasma reproducibility and automated data collection facilitate thorough characterization of the properties of both the fast ions and the background plasma. The apparatus is illustrated in Fig. 1a. The background argon plasma is produced by a 75-cm diameter cathode at one end of the LAPD. The plasma is confined by a uniform 1-kG solenoidal field. At the other end of the device, a source is inserted into the plasma and injects fast ions on orbits that spiral toward the distant cathode. A gridded energy analyzer detects the fast ions at interme-

diate distances from the source.

As illustrated in Fig. 1b, the properties of the source also are characterized on a smaller (0.3-m diameter, 3.6-m long) testbed at the University of California, Irvine (UCI). This testbed is a mirror machine; the ion source is mounted along the axis beyond the field coils in a region with a strong field gradient. Background electrons for charge neutralization of the beam are produced by a filament source. Laser-induced fluorescence (LIF) of the argon ions [2] and an energy analyzer diagnose the ion beam.

The ideal source for this experiment has the following properties.

1. A wide energy range (100-1000 eV) to study the energy dependence of transport.

2. Operation at variable angles with respect to the field, $\chi = \cos^{-1}(v_{||}/v)$ =0-70° and operation in fields up to 4 kG.

3. Milliamp beam current to facilitate observation.

4. Atomic physics that accommodates diagnosis with LIF.

5. Modest energy spread ($< 10\%$), small divergence ($< 3°$), and a 2-mm spot size in one direction in order to measure plasma-induced beam spreading accurately.

6. Modest gas load to minimize beam-neutral collisions.

7. Small overall size to minimize the perturbation of the background plasma; no magnetic materials.

These are demanding requirements. We briefly investigated a compact barium source based on ion emission from a tungsten surface [3] but the beam current was inadequate. We then purchased a commercial RF source from

Veeco Instruments/Ion Tech [4] that is normally used for plasma processing of silicon wafers. This source is a RF Kaufman source [5] with continued proprietary development that extends improvements reported by Reader *et al.* [6]. After modification, the Ion Tech source meets most of the ideal requirements. The most notable deficiency is that operation is limited to angles of $\chi \lesssim 25^\circ$ in a 1-kG magnetic field.

This paper documents the performance of this RF ion-beam source when embedded in a magnetic field. Section 2 describes modifications relative to normal source operation. To minimize the neutral pressure in the experimental chamber, the source is operated at relatively low pressure, which raises the energy of the extracted beam (Sec. 3). Successful operation in a strong magnetic field requires a neutralizing electron current (Sec. 4). The effective angle of the beam χ can be increased by operation in a non-uniform field but this introduces additional complications (Sec. 5). The final section (Sec. 6) discusses possible improvements to the source.

2. Source Description and Basic Operation

The main elements of the source are the gas injector, a quartz discharge tube that is surrounded by a RF coil, and accelerating grids (Fig. 2). The RF power ionizes argon gas in the quartz chamber. Some of the ions that are produced in the RF discharge reach the two grids of the accelerator system. The grid closest to the RF discharge, called the screen grid, is biased positively relative to the cylindrical metal shroud that houses the source. The second grid, called the accelerator grid, is biased negatively. The source normally produces a 3-cm diameter beam. For some experiments, a rectangular mask reduces the beam cross section.

The source is inserted into the LAPD vacuum chamber through a rectangular vertical port (Fig. 3). The source is supported on a 1.5-meter long,

1-inch diameter stainless steel shaft; a chevron seal at the vacuum flange allows the shaft to slide and rotate to alter the vertical position and orientation of the source. For efficient RF power handling, the matching network must be near the discharge chamber but the capacitors in the matching network overheat in vacuum. Accordingly, the matching circuit is mounted in a sealed reentrant box. The vacuum feedthroughs for the electrical connections are mounted on the matching circuit box and the box and the interior of the steel shaft are at atmospheric pressure. In addition, compressed air flows through the shaft to provide further cooling. The entire apparatus presents a large electrical perturbation to the LAPD plasma. To reduce this perturbation, the apparatus is electrically isolated from the vacuum chamber by a teflon flange.

The matching network consists of a 170-pF capacitor that is in parallel with the series combination of a 25-pF capacitor and the source inductance. The shield cable for the RF power is electrically connected to the source can. In this configuration, the source resonance occurs at 18.55 MHz (Fig. 4). Because it is desirable to increase the RF frequency f relative to the electron cyclotron frequency (Sec. 4), the resonant frequency is higher than the nominal operating frequency recommended by the manufacturer of 13.6 MHz.

The DC power supplies that bias the screen and accelerator grids are referenced electrically to the (floating) potential of the source can (Fig. 5). A DC break electrically isolates the RF power. Signals that monitor the source performance are isolated inductively. The RF power is modulated in amplitude to avoid overheating.

Typical signals during operation in the LAPD are shown in Fig. 6. The background plasma is formed by biasing the LAPD anode relative to the cathode. The density increases during this "active" phase of the discharge

and the maximum discharge current reaches 7.2 kA. After the active phase, the density steadily decreases in a plasma "afterglow" phase. Active plasmas are formed at a repetition rate of 1 Hz. Both the LAPD plasma and the source RF discharge are sustained at low power between active pulses. The high-power phase for the RF discharge is initiated when the anode bias is applied and persists 70 ms. If the full power is applied continuously, the source overheats within a minute and ceases to operate. The LAPD plasma and the RF discharge share responsibility for this thermal overload: at the UCI testbed, continuous full-power operation is possible while, at UCLA, the source will restart if the RF is turned off for ten minutes. The purpose of the low-power phase is to maintain an ample supply of seed electrons for the RF discharge, improving source reliability.

In normal plasma-processing operation, a "plasma bridge neutralizer" supplies electrons to maintain charge balance outside the source. Within the source, the positive extracted ion current is balanced by a negative current to the screen grid. Indeed, at the UCI testbed, the electron current to the screen grid is a reliable monitor of the ion current extracted from the source. This is not always the case at the LAPD, however. The dense LAPD plasma often alters the charge and current balance in the source, particularly early in the pulse (when the density is high) or when the source is aligned along the magnetic field ($\chi \simeq 0$) (so external LAPD electrons flow readily into the discharge chamber). Under some conditions with the source parallel to the magnetic field, a beam is transiently extracted even *without* the application of RF power; apparently, some of the gas in the discharge chamber is ionized by the LAPD plasma. Current balance is an important consideration for operation at steep angles of χ (Sec. 4).

The gridded energy analyzer illustrated in Fig. 2 is the principal ion beam

diagnostic. The analyzer housing is usually referenced to the potential of the vacuum vessel. A 0.46-cm diameter mesh with transparency of 29% is biased negatively to ~ -45 V to repel electrons. The collector cup is usually biased positively to ~ 72 V to repel thermal ions and reabsorb secondary electrons. It also is possible to increase the cup bias to > 1 keV to measure the beam energy. The analyzer is usually aligned nearly parallel to the magnetic field, facing the source. At the LAPD, it is mounted on a computer-controlled probe drive to measure two-dimensional planes of the beam profile. Typical signals (with and without RF power) are shown in Fig. 6c. Large negative signals are often observed early in the discharge when the plasma density is large. These signals are independent of source conditions and are probably caused by electrons that "leak through" the repelling mesh when the Debye length is smaller than the openings in the mesh. Later in the discharge, the difference between the with-RF and no-RF signals is caused by the ion beam.

Measurements of the beam profile $\Delta z = 0.32$ m from the source are shown in Fig. 7. For these data, the source is at an angle $\chi = 20^\circ$ with respect to the 1 kG axial magnetic field. The plotted data are from relatively late in the discharge (45 ms) when collisional scattering of the beam by the background afterglow plasma is expected to be negligible. The plane of probe data is acquired twice: once with RF power in the source and once with the RF power off to obtain background signal levels. Without a mask, the beam profile is circular with a FWHM that is about 50% larger than the source aperture (Fig. 7a). Figure 7b show the profile with the rectangular mask in place. At the source, the mask is oriented horizontally but the beam profile rotates as the fast ions spiral along their helical trajectories. The FWHM of the beam profile is about twice as wide as the mask.

Beam divergence depends on several factors. The plasma boundary at

the openings in the screen grid can be convex or concave depending on the grid biases and the plasma potential. The source manufacturer states that maximum collimation is achieved when the current to the accelerator grid is minimized. In a study at the UCI testbed, the divergence of the beam decreases as the RF power is increased (Fig. 8). The divergence also depends on the screen bias. In a LAPD experiment with accelerator bias of -10 V, RF power of 80 W, $\chi = 22°$, and a 0.5-cm wide rectangular mask, the beam width 30 cm from the source is 1.6 cm for a screen bias of 390 V but increases to 2.1 cm for $V_{screen} = 250$ V.

The flat collimating mask employed in these tests has not been optimized. We tested another mask with a 0.16 cm slit in two configurations: with the slit 0.8 cm farther from the source and with the slit 0.8 cm closer to the accelerating grid. (The flat mask is 0.9 cm from the accelerating grid.) With the more distant narrow mask, the source performance was unreliable in the LAPD, perhaps because neutralizing electrons could not reach the screen grid. With the mask close to the accelerating grid, arcing occurred in the presence of a background plasma. In contrast, the flat 0.5-cm wide collimating mask had the desired effect of limiting the cross section of the extracted beam without any adverse impact on source performance.

3. Beam Energy at Relatively Low Pressure

The energy of the beam ions is the sum of the screen grid potential, which biases the RF source plasma above ground potential, and the energy of the ions reaching the grid through the source plasma sheath. The accelerator grid potential serves three functions: as a barrier for background plasma electrons, as an accelerator-decelerator stage to increase the extracted ion current, and as an aid in shaping the plasma meniscus at the screen grid holes which, in turn, is important for beam focusing. The accelerator grid

potential does not change the beam energy.

The beam energy is measured using two techniques. At the UCI testbed, with the source oriented parallel to the field ($\chi = 0$), a ring laser with a variable frequency (manufactured by Coherent) injects axially anti-parallel to the beam. Metastable argon ions in the $3d^2G_{9/2}$ state are excited to the $4p^2F_{7/2}$ state when the Doppler-shifted wave frequency $\omega(1 + v_{\|}/c)$ matches the frequency of the atomic transition, $\delta E/\hbar$. Excited ions subsequently radiate a photon when they relax to the $4s^2D_{5/2}$ state. A mirror placed close to the source collects this fluorescence light. Scanning the laser frequency yields the ion velocity distribution function. The peak of the distribution is shown in Fig. 9a. As expected, the frequency shift increases with increasing screen voltage because the parallel velocity increases. The energy spread of the accelerated beam ions can also be obtained from the measurements; the spread in parallel energy is a few eV in the lab frame. An advantage of the LIF technique is that, in contrast to probe measurements, the diagnostic does not perturb the plasma.

The energy can also be measured by varying the bias voltage on the energy analyzer (Fig. 9b). When the bias voltage exceeds the beam energy, the beam ions are repelled by the collector and the analyzer current drops. The derivative of the analyzer current as a function of bias voltage can be interpreted as an energy distribution of the beam. The maximum derivative is interpreted as the beam energy.

Figure 9c summarizes the various measurements. In one set of LIF measurements, the inferred energy increases linearly with screen voltage for $V_{screen} = 40$-1000 V with a constant energy offset of 130 eV. In another set of measurements, the energy offset increased 35 eV when the gas flow through the source was reduced to $\sim 60\%$ of its previous value. The energy offsets

inferred from the analyzer measurements at the UCI testbed with $\chi = 0$ are similar to the LIF values. The offset increases with decreasing source pressure and with increasing source power (Fig. 9b). With the source at $\chi = 20°$ at the LAPD for the conditions of Fig. 6, the energy offset measured by the analyzer is 80 eV. Similar offsets and energy spreads were previously reported for a capacitive RF source with similar grid structure [7].

Collisions between the beam ions and argon neutrals attenuate and scatter the beam. For our experiments, which are conducted on length scales approaching 10 m, it is important to minimize the neutral pressure in the main chamber. To that end, the source is operated with the lowest gas flow that is compatible with reliable performance. Without a collimating mask, a gas flow of 1.7 sccm is typical. With the collimating mask, the flow can be further reduced to 1.3 sccm, which gives a gas pressure in the LAPD main chamber of 2.3×10^{-5} Torr. These flows are much lower than the manufacturer's recommended flow for plasma processing applications of 6-12 sccm.

The low gas pressure increases the electron temperature T_e in the discharge chamber, which increases the energy offset. This can be understood using the formalism developed by Lieberman and Lichtenberg [8]. The total energy of ions reaching the screen grid from the RF discharge chamber is the sum of the ion energy entering the sheath, which is associated with the Bohm velocity, $E_B = \frac{1}{2}T_e$, and the sheath potential, $V_s = \frac{1}{2}T_e \ln[M/(2\pi m)] = 4.7T_e$. (The mass ratio $M/m = 7.3 \times 10^4$ for argon.) Thus, the total ion energy at the screen grid surface is $E_i = E_B + V_s = 5.2T_e$. Lieberman and Lichtenberg assert that the electron temperature can be estimated by equating the volume ionization to the total ion loss to all surfaces. This yields a transcendental expression for T_e that depends on the gas pressure and the geometry of the discharge chamber. For chamber pressures of 2×10^{-3} Torr, the expected

energy offset is $\sim$ 25 eV, consistent with the manufacturer's claim. However, if the gas pressure is four times lower, the predicted energy offset increases to $\gtrsim$120 eV, which is comparable to the measured offset (Fig. 9b). Evidentally, the reduced gas pressure needed to minimize charge exchange losses of the beam in the main chamber produces a significant upshift of the extracted beam energy.

4. Effect of Magnetic Field

The ion gun performance in various magnetic field configurations was tested at the UCI testbed. To avoid ambiguities due to beam focusing on a collector target during operation at different angles and magnetic fields, the screen grid current was used to determine gun performance. For the testbed conditions, this current is a direct measure of the emitted ion current, since for each emitted ion an electron has to be collected at the screen grid to maintain charge neutrality inside the gun plasma. In Fig. 10, the gun symmetry axis is parallel to the ambient magnetic field ($\chi = 0$). Initially, the screen current increases with increasing magnetic field because a modest magnetic field ($B \gtrsim 10$ G) reduces electron transport and increases the source plasma density. On the other hand, at higher magnetic fields, the cyclotron motion becomes counterproductive. With the cyclotron frequency much larger than the RF frequency and with the RF-induced electric field perpendicular to the magnetic field, the average electron acceleration during one cyclotron orbit becomes small. Increasing the RF power level can partially compensate for this effect (Fig. 10).

When the gun is rotated perpendicular to the field, the gun performance rapidly degrades (Fig. 11a). One factor that influences this degradation is the reduction of the plasma volume that is in contact with the screen grid since the electrons are strongly magnetized at high fields (Fig. 11b). (The electron

gyroradius is ~ 1 mm at 100 G.) This plasma volume becomes considerably larger at low fields where the diameter of the electron cyclotron orbit becomes comparable to the plasma dimensions. Consequently, at $B \sim 20$ G, the screen grid current is essentially the same for $\chi = 0$-$45°$ (Fig. 11a).

Experiments at the LAPD suggest that it is difficult to maintain a neutralizing electron current when the source is at a large angle with respect to the field. In these experiments, stable operation at $\chi = 0°$ is established, then the source is gradually rotated until the source performance is intermittent. Source performance is readily monitored using either the screen current in the LAPD afterglow plasma or the visible light emitted by the discharge chamber. Depending on plasma conditions, intermittent operation occurs at angles between $\chi \sim 20$-$30°$ when $B = 1$ kG. At this angle, modest (~ 10 V) changes in the accelerator bias have a strong effect on source operation. If the accelerator bias is reduced to allow more LAPD plasma electrons into the discharge chamber, the source operates more reliably. If the accelerator bias is increased, the discharge is completely extinguished. Apparently, at large angles in a strong magnetic field, both the plasma electrons and the discharge electrons are too highly magnetized to reach the screen grid, so the current needed to preserve charge neutrality in the source is lost.

4. Use of a Gradient Field

For studies of fast-ion transport, source operation in strong fields ($\lesssim 4$ kG) at steep angles ($\chi \lesssim 70°$) is desirable but, as discussed in the previous section, source performance degrades as B and χ increase. A possible remedy is to create the fast ions in a lower field region at modest χ, then launch them up a field gradient into a higher field region. If the first adiabatic invariant $\mu = v_\perp^2/B$ is conserved ($v_\perp$ is the velocity component perpendicular to $\mathbf{B}$), then the pitch of the fast ions decreases as they move into the higher field

region according to the formula

$$\frac{v_{\|H}}{v} = \sqrt{\frac{B_H}{B_L}\left(\frac{v_{\|L}}{v}\right)^2 - \frac{B_H - B_L}{B_L}}, \tag{1}$$

where the subscripts H and L represent the values in the high and low field regions, respectively. For example, if the field strength is doubled so that $B_H/B_L = 2$ and the initial pitch angle is $\chi_L = 30°$, Eq. 1 indicates that the pitch angle increases to $\chi_H = 45°$.

Figure 12 shows the results of an experiment to test this idea in the LAPD. The current in the field coils at the end of the machine is lowered by a factor of two, while the coil currents in the central portion of the machine are raised slightly. This produces a field of ~ 0.6 kG at the axial position of the source that increases steadily to a value of 1.1 kG 2.2 m away, where the beam is measured. For the conditions of this experiment, the ratio of the gyroradius to the gradient scale length of the magnetic field is $\rho\nabla B/B = O(0.1)$ so, theoretically, the magnetic moment μ is conserved and Eq. 1 is valid. In a uniform field in the absence of collisions, the fast ions spiral on helical orbits. For a source of finite extent, the orbits cross a downstream plane in a pattern that depends on the initial gyrocenters of the orbits and the phase of the gyromotion. The expected pattern is modeled by solving the Lorentz force law $\mathbf{F} = q\mathbf{v} \times \mathbf{B}$ for the ion orbits; the initial positions and velocities are determined by a Monte Carlo routine for assumed values of the source profile and divergence (Fig. 12). In a gradient field, a larger spread in gyrophase is predicted for a source of finite extent. The measured profile in the gradient field is at a position that is close to the expected location and is more elongated in gyroangle than the profiles in a uniform field, as theoretically expected. According to the modeling, the average pitch angle of the beam increases from 22° to 28° for these conditions. Based on the data of Fig. 11, we hoped the beam would become more intense but this is

not observed.

5. Future Improvements

A RF plasma-processing source has successfully produced a $\sim$ 10 mA, 0.2-1.1 keV argon ion beam at an angle of $\chi \simeq 20^\circ$ with respect to a 1 kG magnetic field in the LAPD device. This source is suitable for studies of collisional diffusion of fast ions.

The major limitation of this source is that the pitch angle is presently limited to $\chi \lesssim 25^\circ$. This limit can be relaxed by employing a field gradient, although this tends to increase the spot size of the beam. Increasing the radius of the discharge chamber might enable more electrons to reach the screen grid at larger values of χ (Fig. 11), which might extend the operational range.

The collimating mask could be optimized further for transport experiments. A smaller opening might further restrict the flow of neutral gas into the chamber and reduce the spot size without significantly weakening the extracted beam.

For some experiments, a more intense source is needed. If the pulse duration is shortened, the peak power could be increased without causing overheating.

Acknowledgements

We thank W. Gekelman, V. Laul, D. Liu, S. Vincena, and D. Zimmerman for their assistance. This work was performed at the basic plasma user facility that is supported by NSF/DOE.

References

[1] http://128.97.43.7/bapsf/pages/diagram.html.

[2] G. D. Severn, D. A. Edrich, and R. McWilliams, Rev. Sci. Instrum. **69**, 10 (1998).

[3] HeatWave HWIG-250 ion gun with one #1139-07 barium source.

[4] IonTech 03RF ion source.

[5] H. R. Kaufman, J. J. Cuomo, and J. M. E. Harper, J. Vac. Sci. Technol. **21**, 725 (1982).

[6] P. D. Reader, D. P. White, and G. C. Isaacson, J. Vac. Sci. Technol. **15**, 1093 (1978).

[7] J. Engemann, D. Korzec, K.-P. Ningel, and G. Zrnc, Rev. Sci. Instrum. **63**, 3073 (1992).

[8] M. A. Lieberman and A. J. Lichtenberg, *Principles of plasma discharges and materials processing*, Wiley, New York, 1994.

Figure Captions

Figure 1. (a) Schematic illustration of the apparatus at the LAPD. The ion gun is 15 m from the heated barium-oxide-coated cathode that forms the background plasma. The injected fast ions spiral toward the cathode on helical orbits in the uniform solenoidal field. (The plotted orbit is the projection of the orbit of a 1000 eV argon ion with $\chi = 25°$.) An analyzer on a probe drive measures the beam profile at various distances from the gun. (b) UCI Testbed. The ion gun is outside the field coils of the mirror machine in a region with a flaring magnetic field. The energy analyzer is 0.8 m from the source. A filament creates a low-density background plasma that provides neutralizing electrons for the ion beam. A laser beam is injected along the symmetry axis to excite atomic transitions in fast ions with velocities that satisfy the resonance condition; fluorescence photons are collected by a mirror placed close to the gun.

Figure 2. Schematic diagram of the IonTech RF source. Argon gas bleeds into the quartz discharge chamber where it is ionized by the RF waves. Ion current is extracted through the screen and accelerator grids. An optional aperture mask can alter the beam profile. Electron current to the screen grid helps maintain charge neutrality in the discharge plasma. An energy analyzer with a positively biased collector cup, a negatively biased screen, and a "grounded" screen and shield cap measures the ion beam.

Figure 3. Mechanical installation of the ion source in the LAPD (not to scale).

Figure 4. Input power to the gun and reflected power versus RF frequency during CW operation at relatively low power.

Figure 5. Electrical configuration of the gun.

Figure 6. (a) Line-average electron density from a microwave interferom-

eter located in the middle of the LAPD. The nominal interferometer path length is 75 cm. The active and afterglow phases of the discharge are indicated. (b) Forward power to the ion gun with RF. (c) Energy analyzer signal with (solid) and without (dashed) RF. Conditions: $B = 1$ kG; peak discharge current 7.2 kA; argon chamber pressure 2.3×10^{-5} Torr; screen voltage of 390 V; accelerator voltage of -10 V; rectangular mask; gas flow to gun of 1.33 sccm; $\chi = 22°$; source at $x = 0$ cm and $y = -6$ cm (relative to the symmetry axis); analyzer at $x = 7$ cm, $y = 0$ cm, and axial distance from the source of $\Delta z = 2.24$ m; analyzer biases of -42 V and 72 V.

Figure 7. Contours of energy analyzer signal (in μA) (a) without a mask and (b) with a 0.5 cm by 3.0 cm rectangular mask for the conditions of Fig. 6. The dimensions of the apertures are shown. The background signal in the absence of RF has been subtracted from the data. $\Delta z = 0.32$ m; $t = 45$ ms.

Figure 8. Energy analyzer signal versus horizontal position of the probe in the UCI testbed for various values of the RF power. The inset shows the full-width half-maximum of the profile versus RF power. Screen voltage of 500 V; $B = 1.5$ kG; chamber pressure of 1×10^{-4} Torr; $\chi = 0$; no mask.

Figure 9. (a) Frequency shift of the maximum intensity fluorescence light as a function of screen voltage. Gun parameters: 1.5 sccm gas flow and chamber pressure of 2×10^{-4} Torr; 90 W forward power; -15 V accelerator bias. (b) Current from the gridded energy analyzer versus bias voltage on the collector cup for $V_{screen} = 250$ V for various values of RF power and chamber gas pressure. The vertical lines indicate the inferred beam energy for two of the curves. (c) Beam energy measured by LIF (rectangles) and by the energy analyzer ($\times$). The solid rectangles use the data in Fig. (a). The open rectangles are from other measurements at $V_{screen} = 700$ V, RF power of 70 W, and chamber gas pressures of 2.5 and 4.2×10^{-4} Torr. The point

marked "LAPD" is for the conditions of Fig. 6. The dashed line indicates equality between the screen voltage and the beam energy.

Figure 10. Current to the gun's screen grid as a function of magnetic field in the UCI testbed for various values of RF power. $\chi = 0$; chamber pressure of 5×10^{-4} Torr.

Figure 11. (a) Current to the gun's screen grid as a function of magnetic field in the UCI testbed for various values of χ. RF power of 65 W; chamber pressure of 4×10^{-4} Torr. (b) Illustration of the reduced plasma volume that is in contact with the screen grid when the electrons are strongly magnetized and the source is at an angle of $\chi = 45°$.

Figure 12. Calculated ($\times$) and measured locations of the ion beam in a uniform field and in a gradient field at $\Delta z = 2.2$ m for the conditions of Fig. 6. For the gradient field case, equally spaced contours of the analyzer signal are shown; for the uniform field case, the location of the largest signal is indicated by the $\diamondsuit$ symbol. Parameters for the calculation: Energy=500 eV; $\chi = 21°$; linear field gradient of 0.2 kG/m. The initial distribution employed in the Monte Carlo calculation is also shown.

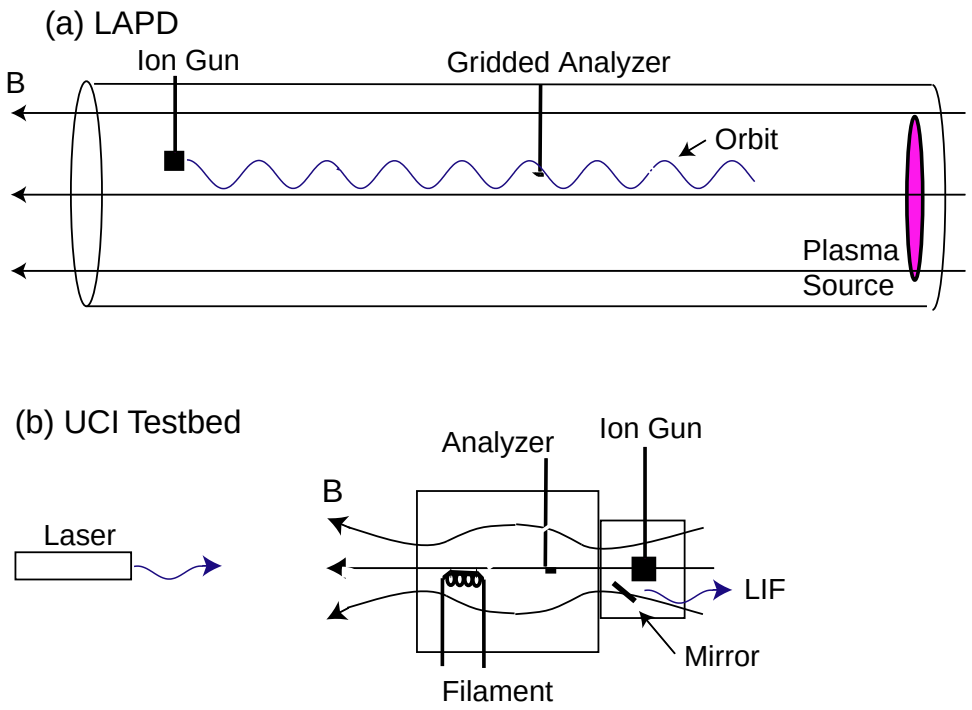

Figure 1. (a) Schematic illustration of the apparatus at the LAPD. The ion gun is 15 m from the heated barium-oxide-coated cathode that forms the background plasma. The injected fast ions spiral toward the cathode on helical orbits in the uniform solenoidal field. (The plotted orbit is the projection of the orbit of a 1000 eV argon ion with $\chi = 25°$.) An analyzer on a probe drive measures the beam profile at various distances from the gun. (b) UCI Testbed. The ion gun is outside the field coils of the mirror machine in a region with a flaring magnetic field. The energy analyzer is 0.8 m from the source. A filament creates a low-density background plasma that provides neutralizing electrons for the ion beam. A laser beam is injected along the symmetry axis to excite atomic transitions in fast ions with velocities that satisfy the resonance condition; fluorescence photons are collected by a mirror placed close to the gun.

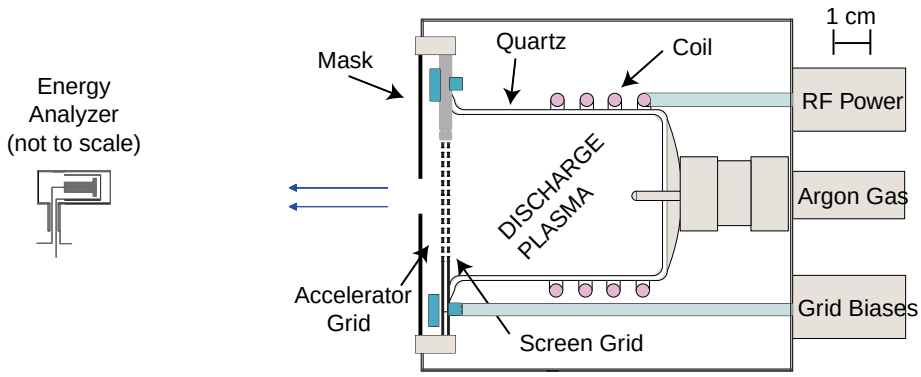

Figure 2. Schematic diagram of the IonTech RF source. Argon gas bleeds into the quartz discharge chamber where it is ionized by the RF waves. Ion current is extracted through the screen and accelerator grids. An optional aperture mask can alter the beam profile. Electron current to the screen grid helps maintain charge neutrality in the discharge plasma. An energy analyzer with a positively biased collector cup, a negatively biased screen, and a "grounded" screen and shield cap measures the ion beam.

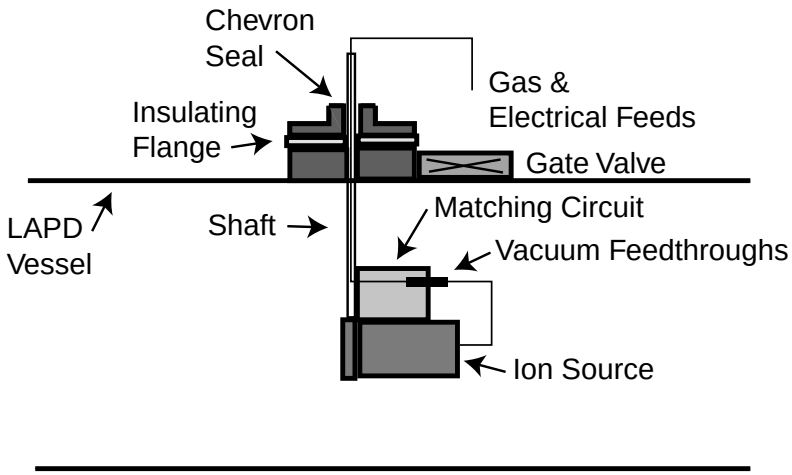

Figure 3. Mechanical installation of the ion source in the LAPD (not to scale).

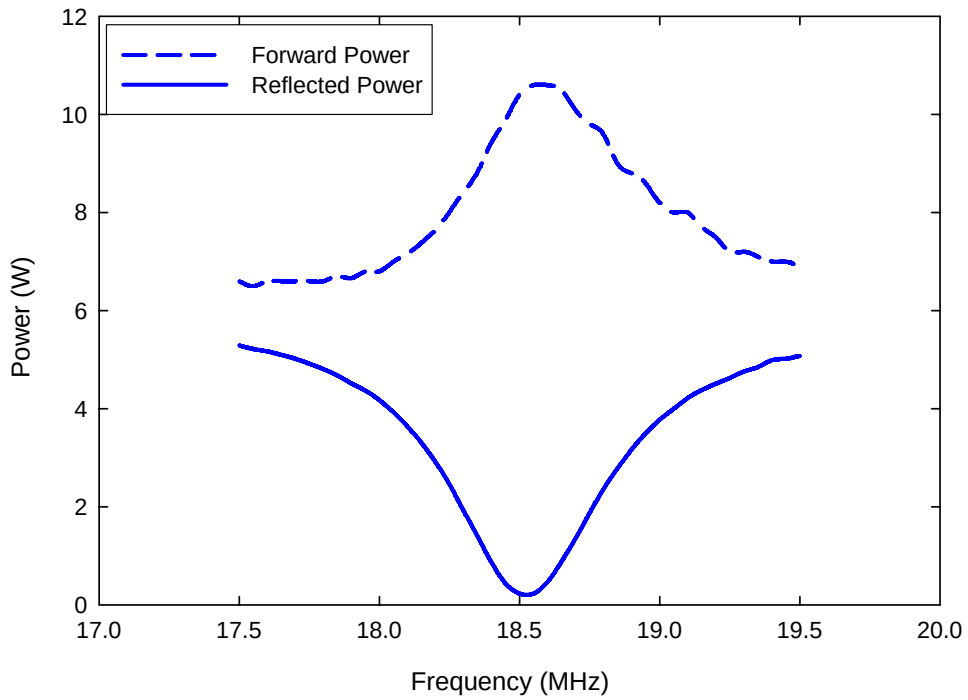

Figure 4. Input power to the gun and reflected power versus RF frequency during CW operation at relatively low power.

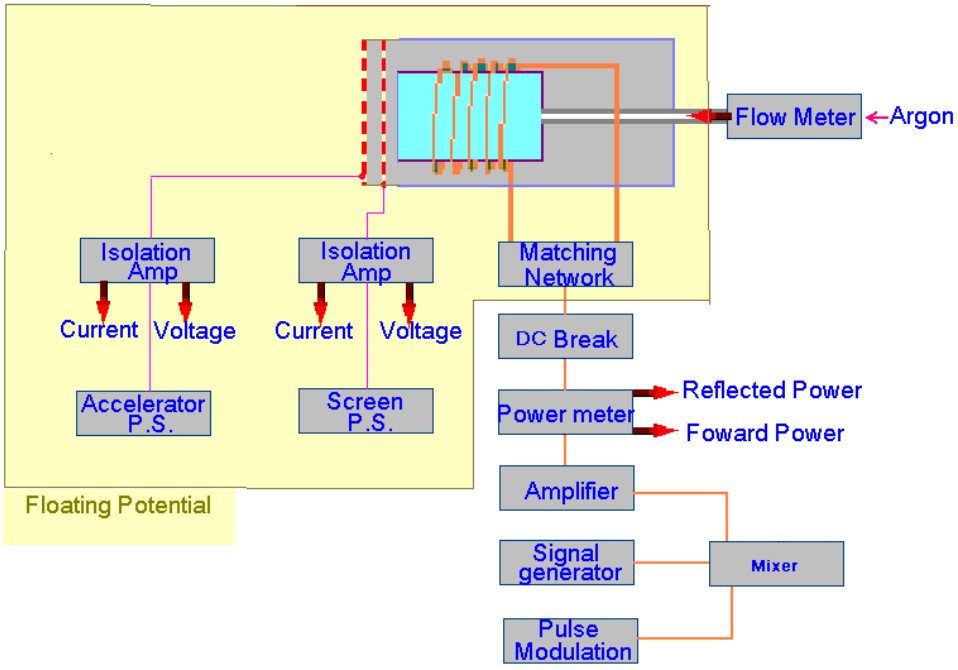

Figure 5. Electrical configuration of the gun.

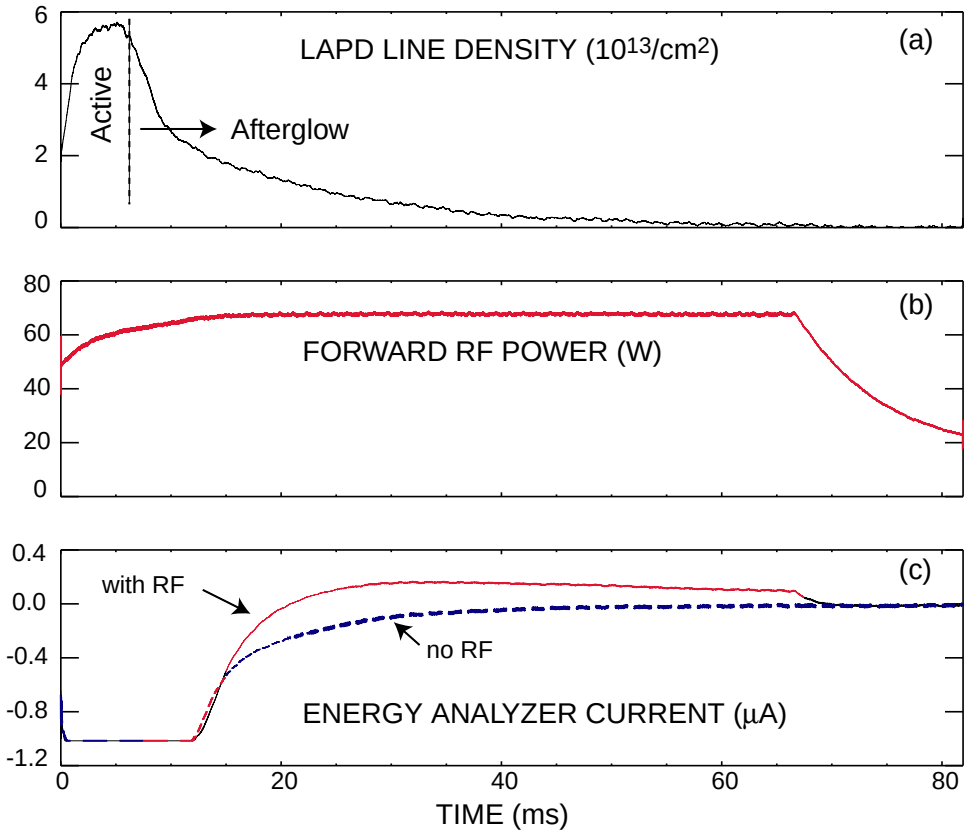

Figure 6. (a) Line-average electron density from a microwave interferometer located in the middle of the LAPD. The nominal interferometer path length is 75 cm. The active and afterglow phases of the discharge are indicated. (b) Forward power to the ion gun with RF. (c) Energy analyzer signal with (solid) and without (dashed) RF. Conditions: $B = 1$ kG; peak discharge current 7.2 kA; argon chamber pressure 2.3×10^{-5} Torr; screen voltage of 390 V; accelerator voltage of -10 V; rectangular mask; gas flow to gun of 1.33 sccm; $\chi = 22°$; source at $x = 0$ cm and $y = -6$ cm (relative to

the symmetry axis); analyzer at $x = 7$ cm, $y = 0$ cm, and axial distance from the source of $\Delta z = 2.24$ m; analyzer biases of -42 V and 72 V.

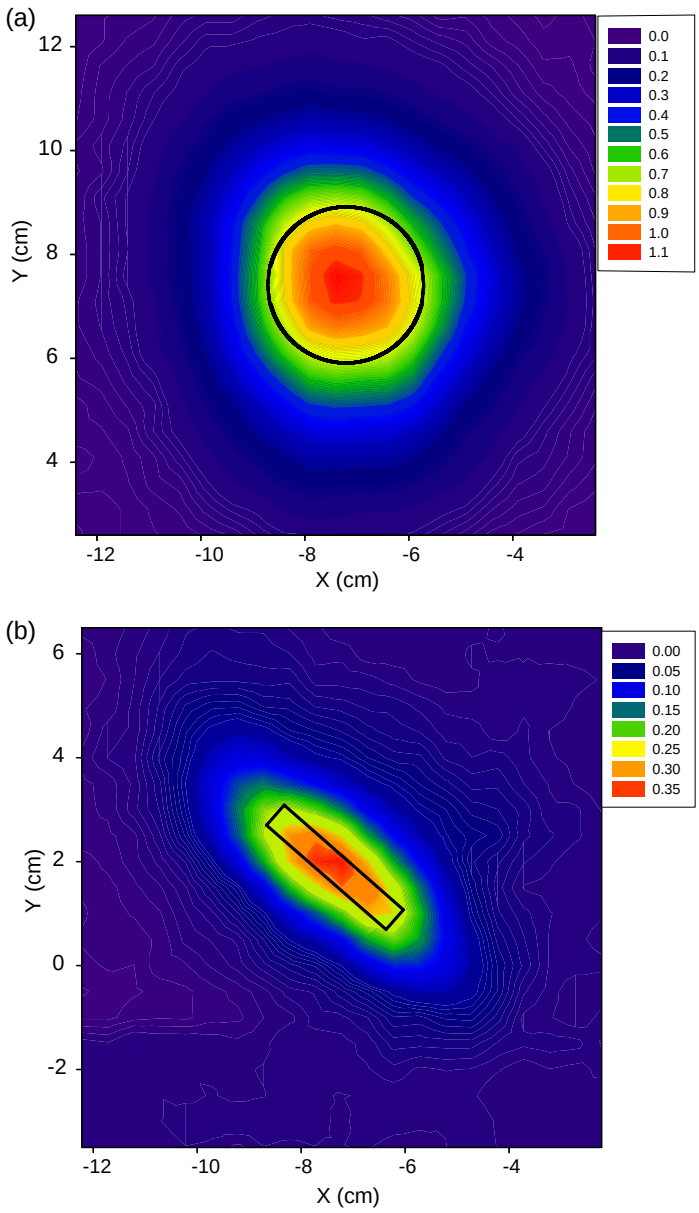

Figure 7. Contours of energy analyzer signal (in μA) (a) without a mask and (b) with a 0.5 cm by 3.0 cm rectangular mask for the conditions of Fig. 6. The dimensions of the apertures are shown. The background signal in the absence of RF has been subtracted from the data. $\Delta z = 0.32$ m; $t = 45$ ms.

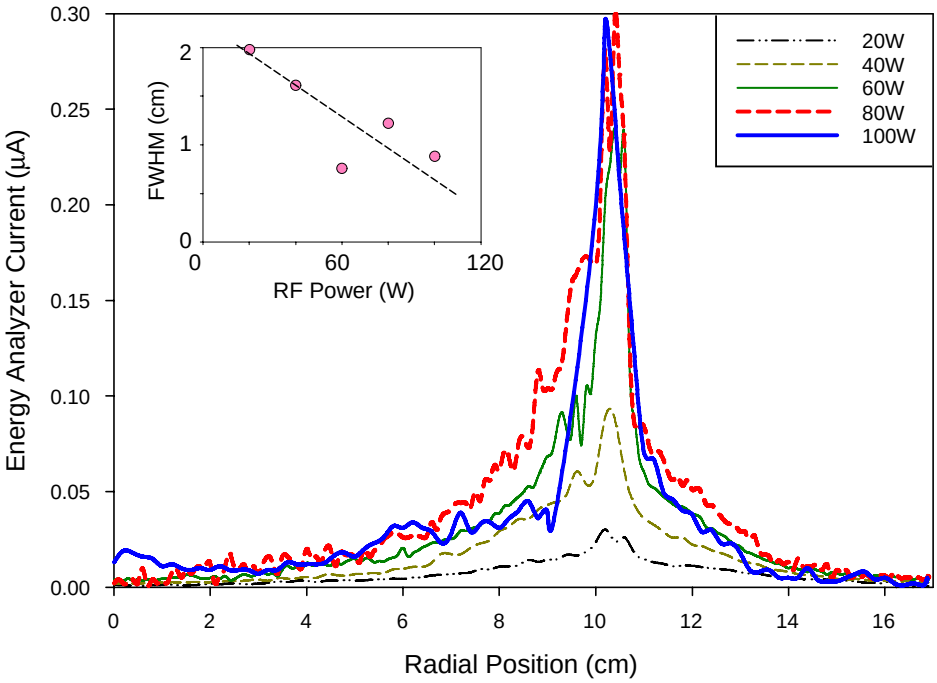

Figure 8. Energy analyzer signal versus horizontal position of the probe in the UCI testbed for various values of the RF power. The inset shows the full-width half-maximum of the profile versus RF power. Screen voltage of 500 V; $B = 1.5$ kG; chamber pressure of 1×10^{-4} Torr; $\chi = 0$; no mask.

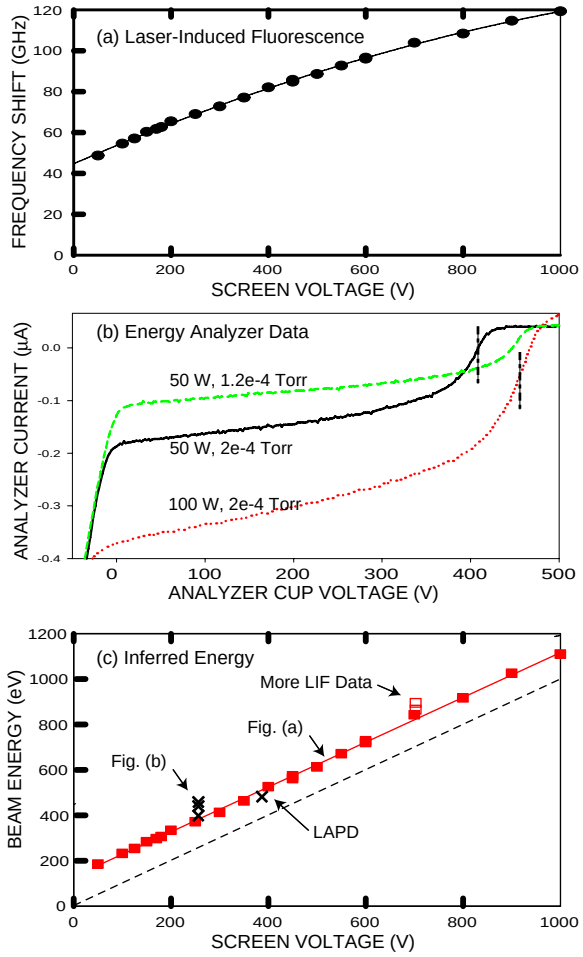

Figure 9. (a) Frequency shift of the maximum intensity fluorescence light as a function of screen voltage. Gun parameters: 1.5 sccm gas flow and chamber pressure of 2×10^{-4} Torr; 90 W forward power; -15 V accelerator bias. (b) Current from the gridded energy analyzer versus bias voltage on the collector cup for $V_{screen} = 250$ V for various values of RF power and chamber gas pressure. The vertical lines indicate the inferred beam energy for two of the curves. (c) Beam energy measured by LIF (rectangles) and by the energy analyzer ($\times$). The solid rectangles use the data in Fig. (a). The open rectangles are from other measurements at $V_{screen} = 700$ V, RF power

of 70 W, and chamber gas pressures of 2.5 and 4.2×10^{-4} Torr. The point marked "LAPD" is for the conditions of Fig. 6. The dashed line indicates equality between the screen voltage and the beam energy.

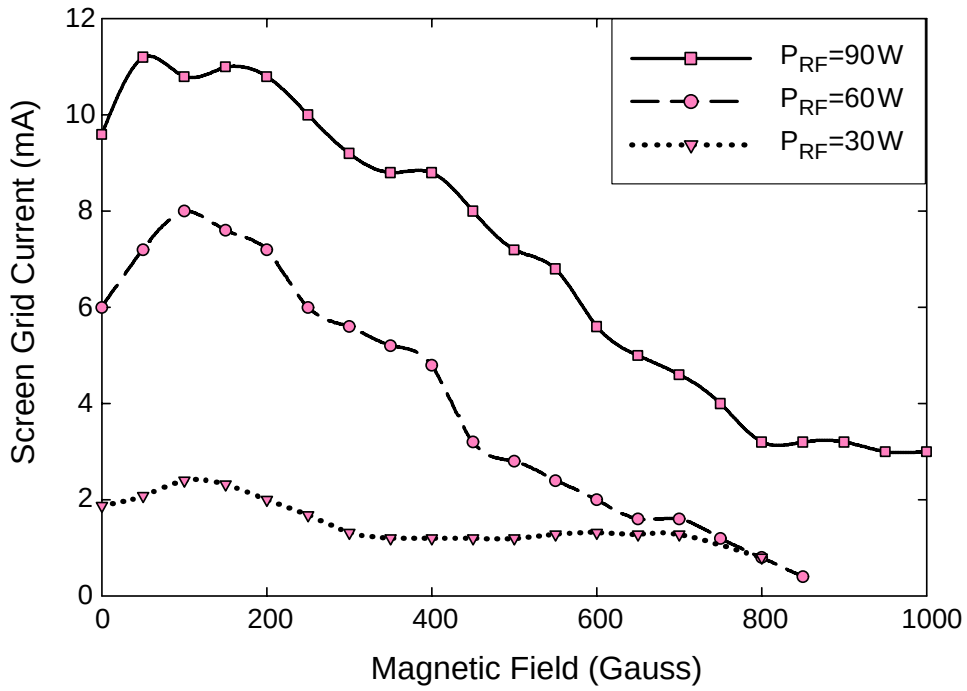

Figure 10. Current to the gun's screen grid as a function of magnetic field in the UCI testbed for various values of RF power. $\chi = 0$; chamber pressure of 5×10^{-4} Torr.

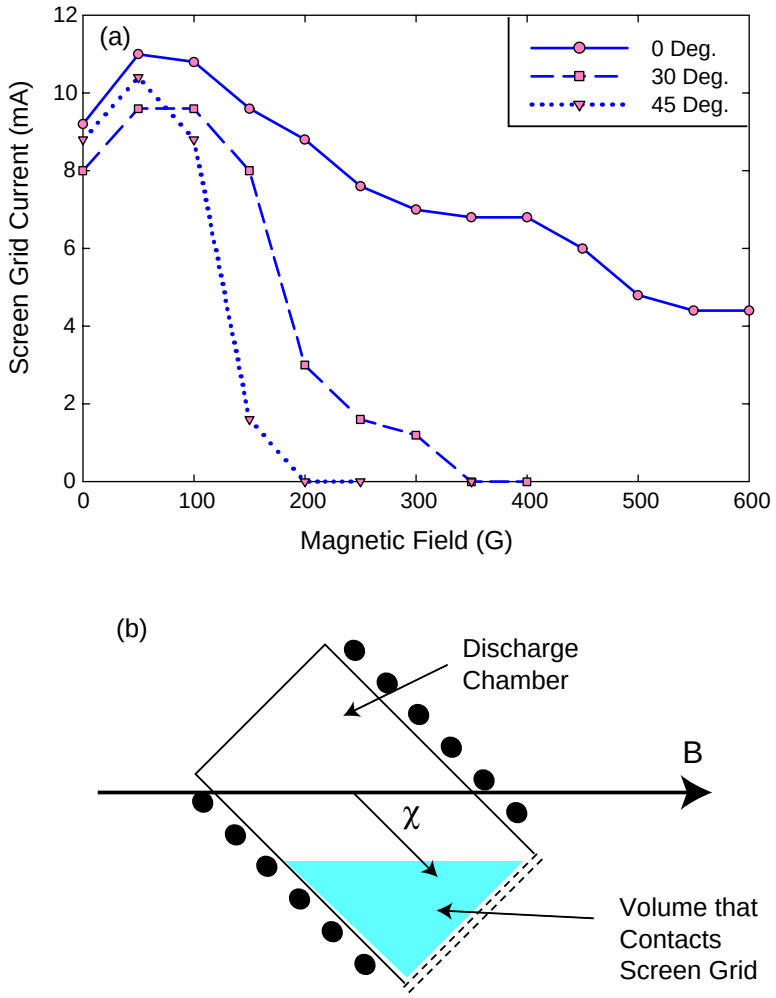

Figure 11. (a) Current to the gun's screen grid as a function of magnetic field in the UCI testbed for various values of χ. RF power of 65 W; chamber pressure of 4×10^{-4} Torr. (b) Illustration of the reduced plasma volume that is in contact with the screen grid when the electrons are strongly magnetized and the source is at an angle of $\chi = 45°$.

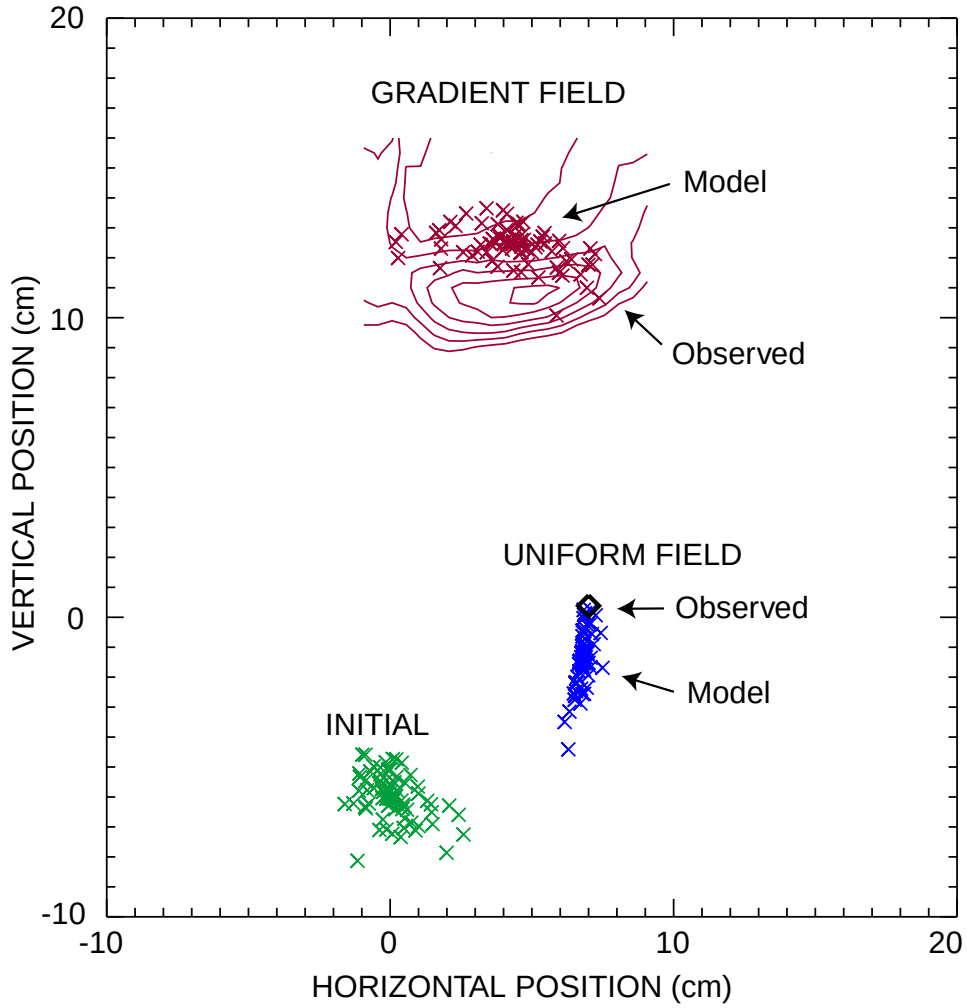

Figure 12. Calculated (×) and measured locations of the ion beam in a uniform field and in a gradient field at $\Delta z = 2.2$ m for the conditions of Fig. 6. For the gradient field case, equally spaced contours of the analyzer signal are shown; for the uniform field case, the location of the largest signal is indicated by the ♢ symbol. Parameters for the calculation: Energy=500 eV; $\chi = 21°$; linear field gradient of 0.2 kG/m. The initial distribution employed in the Monte Carlo calculation is also shown.